Electronic structures and optical and ground-state properties of near-equiatomic Fe-Al alloys

1999 J. Phys.: Condens. Matter 11 8867

(http://iopscience.iop.org/0953-8984/11/45/310)

J. Phys.: Condens. Matter **11** (1999) 8867–8877. Printed in the UK PII: S0953-8984(99)04583-X

Electronic structures and optical and ground-state properties of near-equiatomic Fe–Al alloys

Joo Yull Rhee

Department of Physics, Hoseo University, Asan, Choongnam 336-795, Korea

Received 26 May 1999, in final form 11 August 1999

Abstract. The optical conductivity spectra of $Fe_{1-x}Al_x$ alloys with $x = 0.50$, 0.45 and 0.40 were measured by spectroscopic ellipsometry over the energy range of 1.5 to 5.4 eV. The optical properties change appreciably as the atomic concentration changes. The electronic structures, magnetic moments and the optical conductivity spectra for FeAl, Fe_9Al_7 and Fe_5Al_3 alloys were calculated using the linear-muffin-tin-orbital method within the local spin-density approximation. The spin–orbit interactions were included and the defect-specific supercell method was employed for Fe_5Al_3 and Fe_9Al_7 alloys. Although the calculated ground state for the perfectly ordered equiatomic FeAl alloy was ferromagnetic, the total-energy difference between the ferromagnetic and paramagnetic states is only 0.43 mRyd. The calculated magnetic moment is similar to the previous calculated value for Fe_5Al_3, while it differs significantly for Fe_9Al_7. The so-called λ-fitting, which simulates the effects of the real part of the self-energy in the optical conductivity spectra calculations, markedly improves the agreement between the experiment and theory.

1. Introduction

The intermetallic binary alloy Fe–Al forms a stable B2 phase (cubic CsCl structure) over a wide range of concentration [1]. It is well known that the perfectly ordered equiatomic FeAl alloy is nonmagnetic even at very low temperature. Two related magnetic transition-metal monoaluminides (MTM-Als), NiAl and CoAl, are also known to be nonmagnetic. The stability of the B2 phase and the nonmagnetic character of these monoaluminides are due to the small charge transfer (0.2–0.3 electrons per atom) from Al sites to the MTM sites [2–5]. However, Fe atoms in excess for Fe-rich alloys near stoichiometry substitute for the Al sites and form magnetic clusters with their eight neighbouring Fe atoms, yielding local magnetic moments [6–8]. These Fe atoms substituted at Al sites are called 'antistructure' (AS) atoms. On the other hand, for Al-rich alloys, vacancies appear at the Fe sites up to 52 at.% Al. If the Al concentration is higher than 52%, there exists a mixture of FeAl and $FeAl_2$ [9].

Equiatomic FeAl alloy has been subjected to extensive study not only because of its interesting magnetic properties but also because of its relationship to the other MTM-Als, NiAl and CoAl. The MTM-Als have attracted considerable attention because of their applicability in many fields. They have good corrosion properties and high oxidation resistance, and are excellent candidates for use as high-temperature structural materials, and so forth [10].

There have been many electronic structure calculations. The self-consistent band structure was calculated [3] using the linear-muffin-tin-orbital (LMTO) method in the atomic sphere approximation (ASA). From the calculated band structure, the authors of [3] also obtained the Fermi surface, the positron localization and the imaginary part of the dielectric function (ϵ_2). During the ϵ_2-spectrum calculation, the dipole transition-matrix elements were included.

0953-8984/99/458867+11$30.00

Later, the same method was employed to calculate many physical properties of point defects in slightly off-stoichiometric FeAl alloys [11].

Another ϵ_2-spectrum was calculated by Eibler and Neckel [12]. They used the augmented-plane-wave (APW) method to calculate the band structure and regenerated the wave functions using the hybridized nearly-free-electron tight-binding interpolation scheme to calculate the dipole transition-matrix elements. The calculated ϵ_2-spectrum was quite different from that of reference [3]. Only the 4.7 eV peak (corresponding to the 0.36 Ryd peak of reference [3]) is similar.

Gu and Fritsche [13] have calculated the electronic structures of a few off-stoichiometric FeAl alloys with AS defects. They used the defect-specific supercell method to introduce an AS defect and overcome the difficulties of a single-site approximation [15]. It was found that the eight nearest-neighbour-clustering (NNC) Fe atoms of AS-Fe, as well as the AS-Fe atom itself, play an important role in determining the magnetic moment of the alloys. The calculated local magnetic moments of AS-Fe and its eight NNC-Fe atoms are 2.5 μ_B and 0.6 μ_B, respectively, resulting in a total magnetic moment of 7.3 μ_B for Fe_9Al_7 alloy. This value is in good agreement with the experimental ones of reference [6], in which the AS-Fe atom and its neighbouring clusters have an effective magnetic moment of $\sim$7.8 μ_B, while it is considerably larger than that of reference [7] in which the measured magnetic moments vary from 4 μ_B to 5.4 μ_B depending on the concentration. The magnitude of the local magnetic moment was not sensitive to the size of the supercell [13].

Bogner *et al* [14] performed high-field ^{57}Fe Mössbauer experiments and theoretical band calculations similar to those reference [13] to investigate the magnetic ordering and defect state of the Fe–Al alloys near the equiatomic concentration. Their theoretical results are essentially the same as those of reference [13]. Their calculated ground state for the equiatomic alloy is a ferromagnetic state with $\mu_{Fe} = 0.71\ \mu_B$ and its total energy is only 0.7 mRyd lower than that of the paramagnetic state. However, the experiments reveal that only 25% of the Fe atoms carry a magnetic moment. The discrepancy could be explained by the noncollinear spin ordering and a high density of defects.

Recently, the optical and magneto-optical properties of FeAl alloy thin films were studied experimentally and theoretically [16,17]. Both ordered and disordered thin films were prepared by the flash evaporation technique in a high-vacuum environment (5×10^{-5} Pa). The disordered film was deposited onto a substrate cooled by liquid nitrogen. For ordered films the substrate was heated up to 680 K. The authors observed some significant changes of magnetic, magneto-optical and optical properties upon order–disorder structural transition and explained the changes within the framework of broken lattice symmetry and the structural-defect approach. The results of calculations of the electronic band structure and optical conductivity (OC) showed that large interior parts of the Brillouin zone are involved in the formation of the observed features in OC spectra of the ordered samples [17].

In this paper we report new experimental OC spectra of bulk polycrystalline $Fe_{1-x}Al_x$ alloys with $x = 0.50$, 0.45 and 0.40 obtained using a spectroscopic ellipsometer over the energy range of 1.5 to 5.4 eV. We observed a substantial change of the optical properties with atomic concentration change. Since the magnitude of the calculated ϵ_2 was previously either too small (of the order of 10^{-2} in reference [3]) or too large (of the order of 10^3 in reference [12]), we also calculated the ϵ_2-spectra (or, equivalently, the OC spectra) using the tight-binding (TB) LMTO method. A defect-specific supercell method [13] was employed to calculate the electronic structures of some nonequiatomic alloys. Some ground-state properties, such as the equilibrium lattice constants, density-of-states (DOS) curves and magnetic moments, and OC spectra were calculated. The characteristics of the peak near 4 eV and its evolution upon concentration change will be discussed using the results of the theoretical calculations.

This paper is organized as follows: sections 2 and 3 summarize the experimental and theoretical procedures briefly; section 4 contains the results and discussions of experiments and calculations; and section 5 summarizes the results and concludes this paper.

2. Experimental procedures

The polycrystalline alloy samples were obtained by melting high-purity ($\geqslant$99.99%) Fe and Al pieces in an arc furnace. They were melted together on a water-cooled Cu hearth in an Ar atmosphere. To ensure homogeneity, the alloys were further heat treated at $\sim$1000 K for one week and were cooled slowly. The cooling period takes about a day. The ingot taken out of the furnace had a button shape and it was cut by a low-speed diamond saw to a shape appropriate for optical measurements. It was mechanically polished with a series of alumina powders down to 0.05 μm diameter. The polished sample was then cleaned by means of alternating immersion into acetone and methanol using an ultrasonic cleaner. We used a spectroscopic rotating-analyser ellipsometer, which is described in detail elsewhere [18].

3. Theoretical calculations

The energy band structures were calculated using a scalar-relativistic version of the TB-LMTO–ASA method within the local spin-density approximation (LSDA). For Fe_9Al_7 and Fe_5Al_3 we used the same method as is described in reference [13]. The equilibrium lattice constants were obtained by minimizing the total energy (E_{TOT}) and they were used in the calculations of the magnetic moments, DOS curves and OC spectra. The calculations for all alloys were spin-polarized ones and the spin–orbit interactions were included in the self-consistent iterations, even though the equiatomic FeAl alloy exhibits nonmagnetic properties experimentally. For the exchange–correlation effects we used the LSDA expression of von Barth and Hedin [19]. The calculation for the equiatomic FeAl alloy was made a spin-polarized one for consistency with those for other nonequiatomic alloys. For equiatomic alloys, if we introduce a magnetic moment smaller (larger) than 0.25 μ_{B} in the first iteration, then the self-consistent calculations lead to a paramagnetic (ferromagnetic) state as the iterations repeat. On the other hand, if one of the Al atoms is replaced by an Fe atom (AS-Fe) in the supercell, the magnetic moments are developed for both AS-Fe and its eight NNC-Fe atoms during the self-consistent iterations.

If the magnetization direction is chosen to be in the z-direction in the spin-polarized calculations, the crystal symmetry reduces from cubic to tetragonal. However, the calculational results were almost insensitive to the choice of crystal symmetry, either cubic or tetragonal. Therefore, we calculated the electronic structures in cubic symmetry to save calculation time. The energy eigenvalues at 56, 35 and 56 $\boldsymbol{k}$-points in the irreducible wedge of a reciprocal primitive cell (1/48 of the whole primitive unit cell) for FeAl, Fe_9Al_7 and Fe_5Al_3, respectively, were calculated in the self-consistent iterations. The real-space unit-cell volume ratio is 1:8:4. For the DOS and OC spectra calculations, we used the linear-energy-tetrahedron method [20] with finer meshes of the irreducible wedge. The whole primitive reciprocal cell was divided into $N \times N \times N$ parallelepipeds ($N = 40$, 20 and 32 for FeAl, Fe_9Al_7 and Fe_5Al_3, respectively) and each parallelepiped was further cut into six tetrahedra. Each of the $6 \times N \times N \times N$ tetrahedra has the same volume in this method.

In the OC calculations we assumed only direct transitions, as usual. All of the calculated OC spectra were broadened using an energy-dependent Lorentzian function of width given by $\Gamma(E) = AE^2\ \mathrm{eV}^{-1}$, where $E = \left[E_f(\boldsymbol{k}) - E_i(\boldsymbol{k})\right]$, $E_i(\boldsymbol{k})$ and $E_f(\boldsymbol{k})$ being the initial and final states, respectively, at the same $\boldsymbol{k}$ as for optical transitions. A is a constant and E is in eV. The

broadening simulates the effects of the imaginary part of the quasiparticle self-energy and the instrumental resolution. We set the limit for $\Gamma(E)_{\max} = 2.0$ eV. Since the calculated spectra after broadening have similar shapes to the measured ones while the energy positions of the strong features are different, we applied the real part of the self-energy correction (so-called λ-fitting [21]) to match the energy positions of the strong features of the experimental and theoretical spectra. The effect of changing the excited-state energies $\hat{E}_n(\boldsymbol{k})$ relative to the energies, $E_n(\boldsymbol{k})$, calculated from the ground-state potential is given by [22]

$$\hat{E}_n(\boldsymbol{k}) = E_n(\boldsymbol{k}) + \lambda_{n,\boldsymbol{k}}[E_n(\boldsymbol{k}) - E_{\mathrm{F}}].$$

$\lambda_{n,\boldsymbol{k}}$ has a dependence on n and $\boldsymbol{k}$, and this can be calculated; however, the calculation is very tedious and time consuming [23]. Hence, we assumed $\lambda_{n,\boldsymbol{k}}$ to be independent of n and $\boldsymbol{k}$. A positive (negative) λ has the effect of raising (lowering) the energies of states above and lowering (raising) those below E_{F}; and hence the peaks in the 'bare' excitation spectrum are shifted to higher (lower) energy. Although the above equation was used as a self-energy correction to individual states (following reference [22]), we should be very cautious when interpreting the results, because we are using a rather simplified correction which is being imposed for the purpose of fitting the excitation spectrum. In the correction for the optical conductivity spectra, we are only concerned with the difference of the self-energy corrections, not with the individual initial and final states. Thus a negative λ is likely to arise from a large positive self-energy correction to the initial state and a small (positive) correction to the final state. This is a highly simplified procedure, adopted to avoid the very complicated task of evaluating self-energy corrections for individual states. The corrected OC, $\hat{\sigma}(\hat{\omega})$, is given by

$$\hat{\sigma}(\hat{\omega}) = \frac{1}{1+\lambda}\sigma\left(\frac{\omega}{1+\lambda}\right)$$

where $\sigma(\omega)$ is the uncorrected OC. The self-energy effects, due to the increase of energy of the excited states below the Fermi level relative to the energy calculated from the ground-state potential, may lower the energy position of the calculated structures towards the measured one [22]. It is not difficult to find similar effects [21, 22, 24, 25]. The fitting procedures are described in detail elsewhere [21, 24]. One thing that we should note is that the introduction of the parameter λ does not create any new features in the OC spectrum; it just shifts the whole spectrum to lower or higher energy depending on the sign of λ. It also reduces or enhances the magnitude of the spectrum.

4. Results and discussion

Figure 1 shows the measured OC spectra of the three alloys. The spectrum for $x = 0.5$ is qualitatively similar to a previously measured one [16]; however, there are some differences in several respects.

First, our measured spectrum shows only a broad peak near 4 eV, while in the previous one there are many structures in addition to the 4 eV peak (denoted as 'D' in reference [16]). We did not observe a shoulder near 2.7 eV ('C'). Since the peak near 1.5 eV ('B') is at the spectral limit of our ellipsometer, we cannot say that the structure was not present in our experiment. Second, our measured value of the magnitude of the optical conductivity at 4 eV (5.7×10^{15} s^{-1}) is 78% larger than the previous measurement (3.2×10^{15} s^{-1}). These differences may be explained by the fact that the samples used in the previous measurements were thin films prepared by the flash method and, hence, the OC spectra could be different from those for bulk samples. However, we do not know the precise reason for these differences at present.

The broad peak at 4 eV for $x = 0.50$ moves toward higher energy and gets weaker as x decreases. For $x = 0.40$ there is a very weak, almost indiscernible shoulder at $\sim$5 eV and the

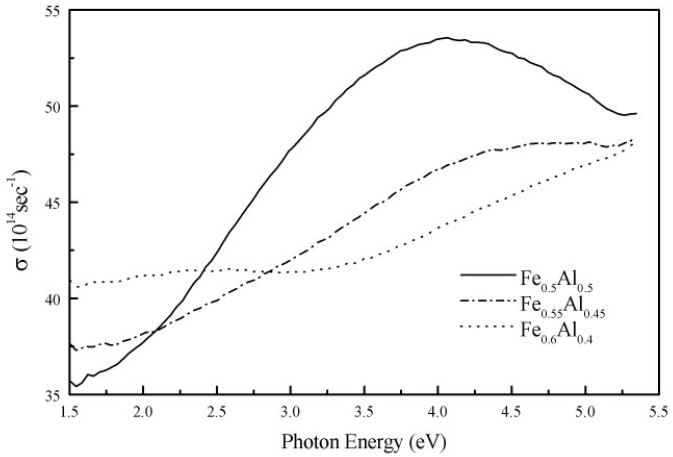

Figure 1. Optical conductivity spectra of Fe–Al alloys. Note that the zero of the optical conductivity is suppressed.

OC increases monotonically with energy, while there is a signature of the emergence of a new structure at around 2.3 eV.

The measured ϵ_2-spectrum (not shown) for $x = 0.50$ shows a weak shoulder centred at around 3.5 eV, which appears as a broad peak in the OC spectrum near 4 eV (see figure 1), while previous calculations show a strong absorption peak at 0.36 Ryd (in reference [3]) or 4.7 eV (in reference [12]). In reference [17] there is a very strong peak near 5 eV in the calculated OC spectrum. All of the aforementioned peaks in the calculated OC spectra are located at higher energy than the measurement and this phenomenon is not rare for the transition metals and their alloys.

To understand the characteristics and evolution of the 4 eV peak upon the concentration change and clarify the discrepancy between experiment and theory, we calculated the electronic structures for FeAl, Fe_9Al_7 and Fe_5Al_3. Various calculational results are summarized in tables 1 and 2 and the parameters used in the so-called λ-fitting are given in table 3.

We will discuss some other calculational results before discussing those from the OC spectra. The equilibrium lattice constants, the DOS at the Fermi level $N(E_F)$, the charge transfer ΔQ and the magnetic moment μ are summarized in table 1.

The equilibrium lattice constants were obtained by minimizing E_{TOT}. We calculated E_{TOT} at several different lattice constants and fitted the E_{TOT}–R_{WS} curve to a parabola, where R_{WS} is the Wigner–Seitz radius. ΔE_{TOT}–R_{WS}, where $\Delta E_{TOT} \equiv E_{TOT} - E_{TOT,min}$, is plotted in figure 2. Since ΔE_{TOT}–R_{WS} curves are shown, the fitted curves touch the zero baseline at the equilibrium R_{WS}. We can easily find the equilibrium lattice constants from the fitting results. The spin-polarized calculations without spin–orbit interactions naturally showed identical results to the spin-unpolarized calculations. The equilibrium lattice constant changes in such a way that the nearest-neighbour distance decreases as the Al concentration, x, decreases. The equilibrium lattice constants are 5.3575 au, 10.6604 au and 10.6292 au, corresponding to values of R_{WS} of 2.6379 au, 2.6244 au and 2.6168 au for FeAl, Fe_9Al_7 and Fe_5Al_3, respectively. The changes in the R_{WS}s are 0.51 % and 0.80% for Fe_9Al_7 and Fe_5Al_3, respectively, with respect to that of the equiatomic CoAl alloy. This trend is the same as in the case of similar calculations for the $Co_{1-x}Al_x$ ($x = 0.5$, 0.4375 and 0.375) alloys [5].

E_{TOT} per atom also decreases as x decreases; -1513.19 Ryd (FeAl) $\rightarrow -1641.79$ Ryd

Table 1. The calculated equilibrium lattice constants, the density of states at the Fermi level $N(E_F)$, the charge transfer ΔQ and the magnetic moment μ for each atomic site. Here 'AS' stands for 'antistructure', 'nn' stands for 'nearest neighbour' and N/A stands for 'not applicable'. For Fe_9Al_7 both experimental and theoretical lattice constants are given.

		Fe_9Al_7		
	FeAl	Calculation	Experiment	Fe_5Al_3
Lattice constant (au)	5.3575	10.6604	10.992	10.6292
E_{TOT}/atom (Ryd)	−1513.19	−1641.79	−1641.79	−1770.40
$N(E_F)$ (states Ryd^{-1}/atom)	18.8640	16.77	17.00	13.2923
ΔQ_{Al} (electrons)	−0.2439	−0.23	−0.18	−0.2556
ΔQ_{nn-Fe} (electrons)	0.2439	0.21	0.17	0.1847
ΔQ_{AS-Fe} (electrons)	N/A	−0.01	−0.01	0.0174
μ_{TOT} (μ_B)	0.00	2.18	5.47	4.0313
μ_{nn-Fe} (μ_B)	N/A	−0.01	0.45	0.5130
μ_{AS-Fe} (μ_B)	N/A	2.24	2.05	2.0832

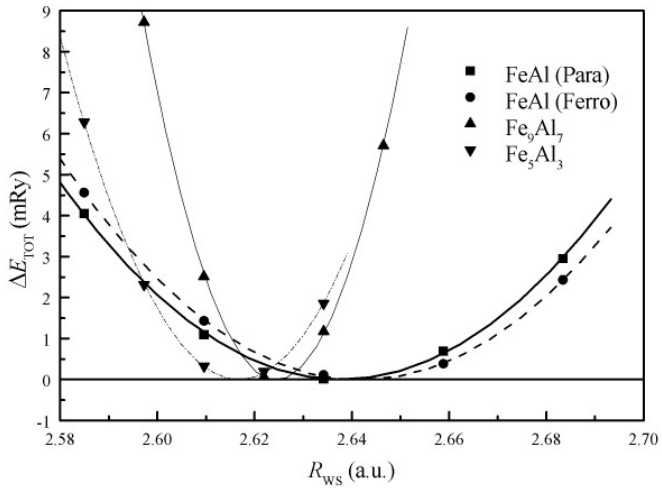

Figure 2. The total-energy difference ($\Delta E_{TOT} \equiv E_{TOT} - E_{TOT,min}$ in mRyd) as a function of the Wigner–Seitz radius (R_{WS}) for equiatomic FeAl (spin-unpolarized and spin-polarized), Fe_9Al_7 and Fe_5Al_3 alloys.

(Fe_9Al_7) → −1770.40 Ryd (Fe_5Al_3). This decrease might be responsible for the contraction of the nearest-neighbour distance with decreasing x.

The calculated DOS curves for three alloys are shown in figure 3. $N(E_F)$ decreases as x decreases (see table 1). The Fermi level is located near the minimum between two strong peaks, corresponding to the bonding and antibonding states of Fe d bands. More precisely, the Fermi level is located at the steeply falling edge of the occupied bonding states and moves toward the minimum as x decreases (FeAl → Fe_9Al_7 → Fe_5Al_3), meaning that the Fermi level shifts to higher energy as x decreases. $N(E_F)$ for equiatomic alloy is 1.39 states eV^{-1}/atom, which is slightly larger than the experimental value of 1.15 states eV^{-1}/atom obtained from the specific heat measurement [26].

The ground state of the perfectly ordered equiatomic FeAl alloy is still controversial.

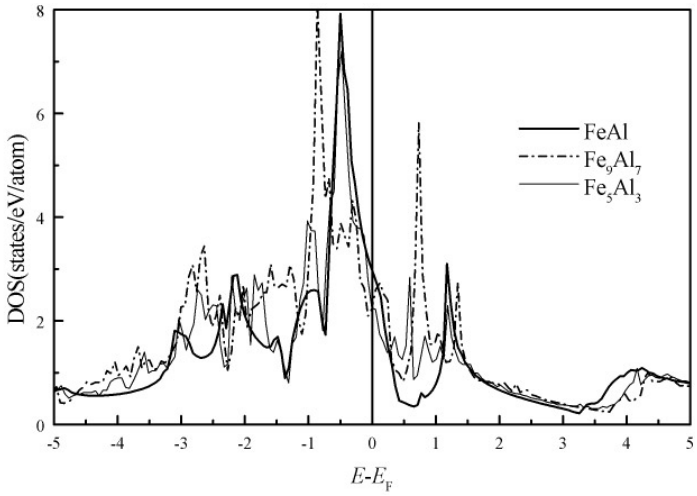

Figure 3. Total-density-of-states curves for FeAl (solid line), Fe_9Al_7 (dotted line) and Fe_5Al_3 (dashed line). The energy scale is relative to the Fermi level.

Gu and Fritsche [13] claimed that the perfectly ordered equiatomic FeAl alloy has a sizable magnetic moment of 0.55 μ_B (the calculation was a spin-polarized one), and E_{TOT} for the ferromagnetic state is slightly higher than that for the paramagnetic state. However, Min *et al* [27] took a different view. They showed that the perfectly ordered, equiatomic FeAl alloy has a naturally converged magnetic moment of 0.55 μ_B from a spin-polarized calculation performed with the equilibrium R_{WS} of 2.87 au, while E_{TOT} for the ferromagnetic phase is lower by 0.7 mRyd. The transformation under pressure from the magnetic to nonmagnetic states occurs in a very narrow range. Bogner *et al* [14] have also found similar results. Sundararajan *et al* [28] also derived similar results to those of Min *et al* [27]. Their calculated magnetic moment was $\sim$0.7 μ_B and the difference in E_{TOT} between the paramagnetic and ferromagnetic ground states was $\sim$0.63 mRyd.

We calculated the electronic structure of the perfectly ordered equiatomic FeAl alloy in two different phases; paramagnetic and ferromagnetic. We also calculated the electronic structure for the paramagnetic phase of FeAl using a spin-polarized calculation, including the spin–orbit iterations. The calculational results for various cases are summarized in table 2. The equilibrium lattice constants were 5.3571 au, 5.3575 au and 5.3653 au for the paramagnetic states without and with spin–orbit interactions and the ferromagnetic state, respectively. As can be seen in table 2, E_{TOT} for the ferromagnetic phase is about 0.43 mRyd lower than that for the paramagnetic one with the spin–orbit coupling. Therefore, we conclude that our calculational results support those of references [14], [27] and [28].

Table 2. Results of various theoretical calculations for the perfectly ordered equiatomic FeAl alloy with the equilibrium lattice constants in various phases. N/A stands for 'not applicable'.

	Paramagnetic		
	No $\boldsymbol{L}\cdot\boldsymbol{S}$ interaction	$\boldsymbol{L}\cdot\boldsymbol{S}$ interaction	Ferromagnetic
Lattice constant (au)	5.3571	5.3575	5.3653
E_{TOT} (Ryd)	−3026.383668	−3026.384165	−3026.384598
μ_{TOT} (μ_B)	N/A	1.5×10^{-3}	0.7175

If the calculation was a spin-polarized one and an initial magnetic moment smaller (larger) than 0.25 μ_B per Fe atom was introduced in the first iteration, then the subsequent iterations led the system to the paramagnetic (ferromagnetic) phase. For the paramagnetic phase the spin-polarized calculation with the spin–orbit interactions produces a lower E_{TOT} than the spin-unpolarized one.

We also calculated the lattice constant for which the magnetic moment was suppressed. The magnetic moment was completely suppressed (less than 1.5×10^{-4} μ_B) when the lattice constant was smaller than 5.07 au, corresponding to the pressure of 0.42 Mbar. We could not compare this result with those of reference [28] because the numerical values of the lattice constant for the complete suppression of the magnetic moment were not given in reference [28] and only the pressure (0.22 Mbar) was given, which is about 52% of our result.

The magnetic moment is 2.24 μ_B for AS-Fe and it is 2.08 μ_B for Fe_9Al_7 and Fe_5Al_3, respectively. The eight NNC-Fe atoms of the AS-Fe atom have about -0.01 μ_B and 0.51 μ_B per atom for Fe_9Al_7 and Fe_5Al_3, respectively—playing an important role in determining the magnetic moments of the alloys. For Fe_5Al_3 the calculational results for the magnetic moments are similar to those from the previous calculations [13], while for Fe_9Al_7 they differ significantly. In the previous calculations the magnetic moments for the NNC-Fe atoms are 0.6 μ_B per atom for both Fe_9Al_7 and Fe_5Al_3 and the magnetic moment is not sensitive to the size of the supercell.

In order to understand the discrepancy between our results and those from previous calculations [13] we calculated the electronic structures for nonequiatomic alloys under various conditions and found the following results. First, since the calculated equilibrium lattice constant is smaller than the experimental ones, we used the experimental one and the results are summarized in table 1. The magnetic moments of the eight NNC-Fe atoms are 0.45 μ_B, which is comparable to the previous value, resulting in a total magnetic moment of 5.47 μ_B per unit cell, while the rest of the calculational results are almost insensitive to the lattice constant. E_{TOT} for the experimental lattice constant is slightly higher than that for the calculated equilibrium one. Second, for lattice constants smaller than the experimental one, not only is E_{TOT} very sensitive to the choice of the ratio of the muffin-tin radius of the Al atom to that of the Fe atom, but so also is the magnetic moment. The calculated equilibrium lattice constants (table 1) are obtained using the same muffin-tin radius for both atoms. If we use the ratio of the radii of free atoms ($R_{MT}^{Al}/R_{MT}^{Fe} = 1.06$), Fe_9Al_7 alloy exhibits no magnetic moment. Therefore, we can conclude that the ratio of the muffin-tin radii—as well as the size of the unit cell—is very important to the theoretical determination of the ground-state properties, such as E_{TOT}, the magnetic moments and the DOS.

We want to point out one more aspect of the calculational results related to the magnetic moments. As mentioned before, it is commonly believed that the non-negligible amount of charge transfer from Al to Fe, i.e. a significant ionic character in the metallic bonding, plays an important role in the stability of these alloys near the equiatomic range [3–5].

The charge transfer is also responsible for the nonmagnetic character of the perfectly ordered equiatomic FeAl alloy. In table 1 it is shown that the charge transfer from Al to Fe in the equiatomic alloy is 0.26 electrons, yielding zero magnetic moment. The charge transfer, from Al to Fe in the equiatomic alloy or to the eight nearest atoms of the AS-Fe atom in Fe_9Al_7 and Fe_5Al_3, keeps decreasing as x decreases: $0.26 \rightarrow 0.21 \rightarrow 0.18$ electrons. However, the charge transfer to the AS-Fe atom is -0.01 and 0.02 electrons for Fe_9Al_7 and Fe_5Al_3, respectively. From these data we can conclude that the local magnetic moment of the Fe atom in the perfectly ordered equiatomic alloy completely disappears because of the compensation of the unpaired spin due to the charge transfer from the Al atom. On the other hand, there is a negligible charge transfer between the AS-Fe atom and its eight NNC-Fe atoms, and the

magnetic moment of the AS-Fe atom is about 2.2 μ_B.

The calculated OC spectra of the equiatomic alloy along with the experimental ones are shown in figure 4. The calculated spectrum of equiatomic FeAl alloy without the broadening is very similar to that of reference [17], exhibiting very strong multiple-peak structures at ∼5.2 eV and 6–8 eV. The shape of our calculated OC spectrum for equiatomic alloy is very similar to that of reference [17]; however, the energy positions of the strong peaks are appreciably higher. The strong peak appears at 5.7 eV in our calculation. Since the experimental lattice constant (5.4962 au [29, 30]) is larger than the calculated equilibrium one, we also calculated the band structures with the experimental lattice constant and found that the smaller lattice constant results in a shift of the unoccupied bands to the higher-energy region and of the occupied band to the lower-energy region. Therefore, the energy difference between the bands involved in the optical transition with the theoretical equilibrium lattice constant is substantially larger than that obtained using the experimental lattice constant, yielding features in the OC spectrum calculated with the theoretical equilibrium lattice constant at positions about 0.5 eV higher. This causes the λ-value to be even larger (see table 3).

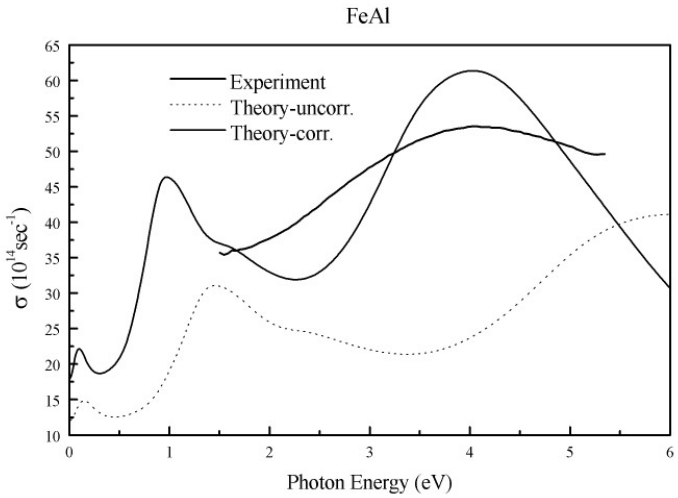

Figure 4. Optical conductivity spectra of equiatomic FeAl alloy. Both self-energy-uncorrected and self-energy-corrected spectra are included. Note that the zero of the optical conductivity is suppressed.

Table 3. Fitting parameters for the real (λ) and imaginary (A and E_{max}) parts of the self-energy.

	FeAl	Fe_9Al_7	Fe_5Al_3
A (eV)	0.05	0.1	0.15
E_{max} (eV)	2.0	2.0	2.0
λ	−0.32	−0.3	−0.18

The multiple-peak structures (peaks above 5.5 eV) merge into a single broad peak after the broadening, having a maximum near 5.8 eV. This peak corresponds to the experimental peak at 4 eV. As can be seen in figure 4, the agreements between the experimental and calculated spectra of the equiatomic alloy are significantly improved by the correction of the real part of the quasi-particle self-energy. Those of the other two alloys also showed similar results (the figures are not shown).

We analysed the characteristics of this peak and found out that they are almost identical to those from the corresponding analysis of the 5 eV peak in reference [17]. The most prominent contributions are (i) near the mid-point of the Γ–X line (Δ symmetry), (ii) near the mid-point of the Γ–M line (Σ symmetry) and (iii) near the M point. The bands involved in the theoretical 5 eV peak are predominantly band 2 (the initial, occupied band) and band 7 (the final, unoccupied band). There are some—but not significant—contributions from bands 3 to bands 8 (near the M point) and from band 1 to band 5 (near the R point). Since the angular momentum characteristics are well analysed in reference [17] and our results are almost the same, we are not going to repeat the discussion in detail here. One thing that we want to mention is that the Al s or p characters of the occupied states are important to this peak.

Our measurements show that the 4 eV peak moves toward higher energy and becomes weaker as x decreases. The multiple-peak structure near 6 eV in the calculation moves towards the higher-energy range and reduces in magnitude as x decreases. This phenomenon is closely related to the fact that the equilibrium R_{WS} decreases as x decreases, resulting in a larger energy difference in the optical transitions due to the shift to higher (lower) energy for the unoccupied (occupied) bands.

Although our measurements did not show the structure at 1.5 eV observed in the previous measurements [16, 17] because of the spectral limit of our ellipsometer, there is a signature of the emergence of a new structure centred at around 2.3 eV in the OC spectrum of $Fe_{0.6}Al_{0.4}$ alloy. It is clearly seen in the calculational results. The 1.5 eV peaks in the broadened and λ-fitted theoretical spectra of the alloys move towards higher energy as x decreases. As pointed out in reference [17], the structure of the OC spectrum in the infrared region is mostly determined by the interband transitions within the t_{2g} manifolds separated by a 'pseudogap'. The 'pseudogap' is caused by the nearest-neighbour atoms (Al) of the Fe atom [31] and the Fermi level is located in the 'pseudogap'. The unoccupied states involved in the 1.5 eV peak for the OC spectrum of the equiatomic FeAl alloy are about 0.5 eV above the Fermi level. Therefore, the energy position and/or the characteristics of the wave function of the unoccupied t_{2g} manifold are sensitive to the structural defects, resulting a shift of the peak to the higher-energy region as x decreases; that is, the defect concentration increases.

5. Conclusions

We measured OC spectra of $Fe_{1-x}Al_x$ alloys with $x = 0.50$, 0.45 and 0.40 using a spectroscopic rotating-analyser ellipsometer over the energy range of 1.5 to 5.4 eV. The OC changes significantly as the atomic concentration changes. A broad peak at 4 eV was observed for $x = 0.50$ and it moves toward higher energy and gets weaker as the Al concentration decreases. The emergence of a new structure centred at around 2.3 eV for $x = 0.40$ in experiments was clearly seen in the calculations. Calculating the OC spectra with the inclusion of the real part (λ-fitting) and the imaginary part (energy-dependent Lorentzian broadening) of the quasiparticle self-energy corrections markedly improves the agreement between the experiment and the theory. The supercell method was used to calculate the magnetic properties of slightly off-stoichiometric alloys and the calculated magnetic moments are in reasonable agreement with the experimental values. The size of the charge transfer between the Fe and Al atoms (usually Al → Fe) is responsible for the local magnetic moments of the Fe atoms at various sites and the stability of the B2 phase of these alloys.

Acknowledgments

This work was supported by the Korea Science and Engineering Foundation through project number 97-0702-01-01-3. Some of the theoretical work was done using a CRAY C-90 supercomputer at SERI, Korea.

References

[1] Singh D 1994 *Intermetallic Compounds* vol I, ed J H Westbrook and R L Fleisher (New York: Wiley)
[2] Okochi M and Yashigawa K 1982 *J. Phys. Soc. Japan* **51** 1166
[3] Koenig C and Kahn M A 1983 *Phys. Rev.* B **27** 6129
[4] Müller Ch, Wonn H, Blau W, Ziesche P and Krivitskii V P 1979 *Phys. Status Solidi* b **95** 215
[5] Rhee J Y, Kim K W, Kudryavtsev Yu V and Lee Y P 1999 *J. Korean Phys. Soc.* **35** S578
[6] Caskey G R, Franz J M and Sellmeyer D J 1973 *J. Phys. Chem. Solids* **34** 1179
[7] Domke H and Thomas L K 1984 *J. Magn. Magn. Mater.* **45** 305
[8] Kuentzler R 1983 *J. Physique* **44** 1167
[9] Paris D and Lesbats P 1978 *J. Nucl. Mater.* **69+70** 628
[10] Fleisher R L, Dimidick D M and Lipsitt H A 1989 *Annu. Rev. Mater. Sci.* **19** 231 and references therein
[11] Koch J M, Stefanou N and Koenig C 1986 *Phys. Rev.* B **33** 5319
[12] Eibler R and Neckel A 1980 *J. Phys. F: Met. Phys.* **10** 2179
[13] Gu Y M and Fritsche L 1992 *J. Phys.: Condens. Matter* **4** 1905
[14] Bogner J, Steiner W, Reissner M, Mohn P, Blaha P, Schwarz K, Krachler R, Ipser H and Sepiol B 1998 *Phys. Rev.* B **58** 14 922
[15] Koch J M and Koenig C 1987 *Phil. Mag.* **55** 359
[16] Kudryavtsev Yu V, Nemoshkalenko V V, Lee Y P and Kim K W 1997 *J. Appl. Phys.* **82** 5043
[17] Antonov V N, Krasovska O V, Krasovskii E E, Kudryavtsev Yu V, Nemoshkalenko V V, Yavorsky B Yu, Lee Y P and Kim K W 1997 *J. Phys.: Condens. Matter* **9** 11 227
[18] Rhee J Y 1992 *PhD Thesis* Iowa State University
[19] von Barth U and Hedin L 1972 *J. Phys. C: Solid State Phys.* **5** 1629
[20] Jepsen O and Andersen O K 1971 *Solid State Commun.* **9** 1763
[21] Rhee J Y, Harmon B N and Lynch D W 1997 *Phys. Rev.* B **55** 4124
[22] Janak J F, Williams A R and Moruzzi V L 1975 *Phys. Rev.* B **11** 1522
[23] Kulikov N I, Alouani M, Khan M A and Magnitskaya M V 1987 *Phys. Rev.* B **36** 929
[24] Rhee J Y, Harmon B N and Lynch D W 1996 *Phys. Rev.* B **54** 17 385
[25] Laurent D G, Callaway J and Wang C S 1979 *Phys. Rev.* B **20** 1134
[26] Okamoto H and Beck P A 1972 *Monatsh. Chem.* **103** 907
[27] Min B I, Oguchi T, Jansen H J F and Freeman A J 1986 *J. Magn. Magn. Mater.* **54** 1091
[28] Sundararajan V, Sahu B R, Kanhere D G, Panat P V and Das G P 1995 *J. Phys.: Condens. Matter* **7** 6019
[29] Taylor A and Jones R M 1958 *J. Phys. Chem. Solids* **6** 16
[30] Müller Ch, Blau W and Ziesche P 1983 *Phys. Status Solidi* b **116** 561
[31] Fu C L 1995 *Phys. Rev.* B **52** 3151